Title

Ligand-Sensitized Lanthanide Nanocrystals: Merging Solid-State Photophysics and Molecular Solution Chemistry

Journal

Inorganic Chemistry, 55(20)

ISSN

0020-1669

Authors

Agbo, Peter
Abergel, Rebecca J

Publication Date

2016-10-17

DOI

10.1021/acs.inorgchem.6b00879

Peer reviewed

Ligand-Sensitized Lanthanide Nanocrystals: Merging Solid-State Photophysics and Molecular Solution Chemistry

Peter Agbo[1] and Rebecca J. Abergel[1]*

[1]Chemical Sciences Division
Lawrence Berkeley National Laboratory
Berkeley, CA 94720, USA
*corresponding author

Abstract

To date, the breadth of scientific research that has been devoted to investigating the photochemical and photophysical behavior of the lanthanide elements has generally fallen into one of two camps: solution studies of luminescent lanthanide metal-ligand complexes or investigations of solid-state nanoparticles, composed primarily of or doped with, lanthanide lumiphores. In the latter case, most research of lanthanide nanocolloids has precluded any investigations regarding the use of organic ligands to overcome the difficulties associated with f-f excitation of lanthanides. Instead, most work on condensed-phase lanthanide luminescence has centered on strategies such as d-f charge separation in divalent lanthanides and the sensitization of lanthanide excited states using quantum dots. Current work now aims at bridging the camps of condensed-phase lanthanide photophysics and the solution chemistry of ligand-lanthanide molecular complexes. Recent efforts have partly focused on the fundamental characterization of $NaGd_{1-x}Ln_xF_4$ nanoparticles featuring surface display of the sensitizer ligand 3,4,3-LI(1,2-HOPO), showing these structures to be capable of converting absorbed ultraviolet light into luminescence from Eu^{3+} and Tb^{3+} ions. These results suggest such use of ligand sensitization as a tool of choice to overcome the constraints of UV solar spectrum/semiconductor band-gap mismatch and low absorption cross-sections in solid-state lanthanide systems.

Introduction

Our current understanding of the periodic table's f-block marks the result of decades of research pursued by scientists of various stripes: from chemists to materials scientists, physicists and biologists. As a consequence, the modern scientific catalog of understood phenomena arising either directly or indirectly from lanthanide chemistry and electronic structure is expansive, ranging from multi-photon up- and down-conversion processes[1–16], to ligand-lanthanide chelation thermodynamics in solution[17–20], to lanthanide binding and efflux mechanisms in biological systems[21–28]. In particular, it has become both widely accepted and abundantly clear that the diversity in the f-orbital electronic structures of the lanthanide elements makes them prime candidates for various possible applications in optoelectronic devices, deep-tissue imaging and luminescence sensing[10,29–32,23,8,33]. Interest in these applications provides much of the motivation driving both applied and fundamental research in lanthanide photochemistry.

Molecular Solution Chemistry of Lanthanides

With respect to their possible photonic applications, the bulk of photochemical literature of the lanthanides has involved work on either molecular complexes, nanocrystalline forms of lanthanides, or glasses where emissive lanthanides occur as either doped or primary constituents[1–3,9,10,34–39]. In the case of molecular complexes, lanthanide luminescence is typically interrogated through the photo-sensitization of lanthanide excited states using organic ligands[9,23,40]. The employ of this “antenna” effect has the benefit of yielding lanthanide excited states with far greater efficiency than generally possible through direct, intra-band pumping of f-levels, a partial result of the generally high molar absorptivities of organic/aromatic ligands (~

10^3-10^5 M^{-1} cm^{-1}). This process stands in stark contrast to the relatively dismal absorption coefficients observed for the direct excitation of most lanthanide transitions (~ 1-10 M^{-1} cm^{-1}), a consequence of the symmetry forbidden and, in some cases, spin-forbidden nature of intraconfigurational f-transitions present in these elements. Sensitization of lanthanides in molecular complexes has also been achieved through the construction of heteronuclear, bi-metallic ligands, intricate ligand constructs capable of discriminating between a d-block transition metal and a lanthanide at distinct binding sites[33,41,42]. There, excitation of a transition metal featuring orbitals overlapping with either bridging ligand states or lanthanide-centered states allows for energy transfer to the f-element with subsequent emission by the lanthanide. However, rational development and successful solution assembly of these molecular complexes requires an understanding of lanthanide chelation chemistry. The shielding of f-electron density by filled 6s and 5p levels in these atoms result in metals that behave predominantly as hard acids, with binding that is primarily ionic, rather than covalent, in character. As hard-soft acid-base (HSAB) theory would predict, these hard, cationic cores are most susceptible to binding by hard donor (base) anionic ligands, explaining the prevalence of oxygen donor atoms in most lanthanide chelators and macrocyclic ligands[17–19]. Solution thermodynamics have played a major role in the quest to develop efficient lanthanide-sensitizing ligands suitable for a variety of applications that utilize f-element properties in the presence of multitudes of additional components such as other metal ions, small organic compounds, or biological macromolecules. Attempts to form stable luminescent complexes range from the insertion of simple carboxylate groups onto chromophore-bearing multidentate scaffolds to the use of dye-functionalized dipicolinic acid derivatives or cyclen-based ligands (DOTA,

DO3A)[43,44], to the synthesis of multidentate ligands incorporating aromatic chelating units such as the sensitizing 2-hydroxyisophthalamide or hydroxypyridinone[45]. Macrocyclic and octadentate ligands have displayed the highest affinities towards lanthanide ions in solutions with complex stability constant ($\log\beta_{110}$) values nearing or exceeding 25, making them most relevant for solution-based applications such as fluorescence-based biological assays[46].

Solid-State Photophysics of Lanthanides

The direction of research on solid-state glasses and nanocolloidal lanthanide systems has largely been governed by a desire to understand and utilize the photophysical traits of these elements. Studies of luminescence behavior in nanoparticulate systems have been especially progressive, with much of the work being geared towards the development of multi-photon conversion for applications in solar energy utilization[3,4,10]. Extracting spectroscopic information from such systems has often demanded the use of laser excitation sources for generating lanthanide luminescence, as their much higher power densities relative to lower-intensity, conventional halogen or arc lamp sources allow for circumventing the issues associated with the low luminescence yields of f-f absorption. Higher efficiency lanthanide emission in solid media has also been achieved through lanthanide sensitization by d-block metal ions as co-dopants and the recent achievement of lanthanide substitution in ZnS and CdS quantum dots[35,36,47]. This latter scheme leverages the very high absorption coefficients that have been found for metal-chalcogen quantum dots, with the host lattice sensitizing the lanthanide dopant.

Lanthanide sensitization by organic ligands typically proceeds through either Forster energy transfer, Dexter energy transfer, or a combination of the two[33]. In the case of Forster

transfer, energy is relayed through the dipolar coupling between the triplet excited state of some donor ligand and the 4f orbitals of a lanthanide acceptor. In the limit of pure Dexter transfer, energy flow between a donor and acceptor proceeds through the initial population of the donor excited state, followed by transfer of the excited electron onto the acceptor atom[48]. A second (or concerted) exchange then occurs from the acceptor's ground state to the donor's ground state. Relaxation of the electron occupying the acceptor excited state back to ground restores the system to its initial configuration. Forster transfer is primarily a through-space interaction, marked by a strong dependence on spectral overlap between the donor luminescence profile and the acceptor absorption spectrum. As a result, this mode of energy transfer generally occurs over several tens of angstroms, with a transfer efficiency governed by:

$$\eta = \frac{1}{1+\left(\frac{r}{r_0}\right)^6} \qquad \text{(equation 1)},$$

where η is the energy transfer efficiency, r is the donor-acceptor distance, and r_0, the Forster distance, is defined as the distance yielding a 50% transfer efficiency[48].

The relatively generous distance dependence observed for Forster energy transfer runs contrary to the Dexter mechanism, where energy transfer is restricted to donor/acceptor distances of ~ 5 Å or less. This limitation of the Dexter formalism is a natural consequence of its dependence on electron exchange. Rapid charge transfer between a donor and acceptor is best facilitated via through-bond interactions – the physical overlap of donor and acceptor orbital wavefunctions – which have persistence lengths of only a few angstroms. The result is an energy

transfer mechanism displaying a rate-distance dependence that corresponds with the semiclassical Marcus model of electron transfer:

$$k = A exp\left(-\beta\left[r - r_o\right]\right) \quad \text{(equation 2).}$$

Here, k is the electron transfer rate. β, with units of inverse length, is a medium-dependent property describing the tunneling distance decay of an electron between donor and acceptor. Terms r and r_0 retain their earlier definitions[49]. As a consequence of eq. (2), Dexter transfer will have minimal contributions between energy transfers in dilute solutions but may become the dominant channel for energy transfer between a donor and lanthanide acceptor in condensed phases, particularly when donor/acceptor spectral overlap is poor.

Nanoparticle research has also focused on modulating lanthanide emission through judicious choice of host lattice; transition probabilities are significantly improved when embedding lanthanides in hosts featuring small phonon energies and low-symmetry (in particular, non-centrosymmetric) metal coordination sites, explaining the prevalence of rare-earth fluoride hosts, particularly the $NaGdF_4$ and $NaYF_4$ crystal systems, in luminescent nanoparticle research. [50–57]. Such sites are capable of breaking f-orbital symmetry and promoting inter-orbital mixing, relaxing the conditions for f-f transitioning. In principle, such changes should result in both higher absorption coefficients and more intense luminescence lines, from the metals.

Bridging Fields

Translating the advances made by researchers in these two camps into projects combining the best aspects of these disparate approaches seems an intuitive direction in which to take

research in lanthanide photophysics. However, the amount of literature on the subject of utilizing ligand sensitization in solid-state lanthanide structures remains relatively small[7,13,15,44,46,52,56,58–68]. The most prominent work produced in this vein include the first ever report of lanthanide nanocrystal sensitization in the IR using tropolonate ligands[68] and a 2012 finding by Zou et. al demonstrating the first example of two-photon up-conversion luminescence in β-$NaYF_4$:Er:Yb nanocrystals, with initial infrared light absorption through an organic ligand[52]. Despite the promise of this strategy for achieving higher total quantum yields for lanthanide lumiphores, the body of scholarship in this area has remained remarkably small since Zhang et. al's first report in 2007[68]. The persistence of this interdisciplinary gap between solution chemists and materials scientists/physicists studying lanthanides becomes even more remarkable considering the standing precedent for the role ligand sensitization has played in other areas of solid-state chemistry and physics – with the maturing field of dye-sensitized semiconductor solar cells serving as perhaps the best example[69].

The current research efforts in our group have been adopted while keeping this disparity in mind. Recent work has involved the investigation of luminescence in $NaGd_{(1-x)}Eu_xF_4$ and related nanoparticles surface-functionalized with the ligand 3,4,3-LI(1,2-HOPO), an octadentate chelator consisting of a linear spermine backbone derivatized with hydroxypyridine-2-one moieties[70]. The project's conception was partly inspired by projects out of the Abergel group in which the photophysical behavior of f-elements complexed by 3,4,3-LI(1,2-HOPO) in solution were studied[18,19,71]. This ligand, which displays very high thermodynamic stabilities for

lanthanide complexation in aqueous solutions ($\log\beta_{110}$ = 20.2 for the $[Eu^{III}(3,4,3\text{-LI(1,2-HOPO)})]^-$ complex)[19], has been shown to be especially adept at sensitizing Eu^{3+} emission, a feat facilitated by spectral overlap of the ligand's triplet state (centered around 19,000 cm^{-1}) with europium's ^5D_J states (Figure 1)[71,72]. The appeal of sensitization in a nanoparticle host featuring low phonon energies also promises to help solve the issues associated with non-radiative solvent quenching of luminescent metal ions commonly found in molecular complexes, as the majority of Eu^{3+} ions in nanocrystalline structures reside in the nanoparticle bulk and are thus shielded from interactions with solvent. Following an initial demonstration of europium luminescence enhancement in these structures by factors of roughly 5000 fold, we have now focused our efforts on optimizing this system and further characterizing its photophysics.

Characterization & Material Optimization

Optimizing the Ligand:Nanoparticle Ratio

As a follow up to our initial characterizations of rare-earth fluoride nanoparticles modified with 3,4,3-LI(1,2-HOPO), we studied the dependence of europium emission on ligand:nanoparticle ratios. Briefly, samples of nanoparticles at concentrations of 0.9 mg mL^{-1} were incubated with varying concentrations of the ligand, spanning from 75 nM to 75 mM. Following overnight incubation at 75 ^oC and the removal of excess ligand through repeated wash cycles in ethanol, nanoparticle luminescence was measured (Figure 2). These data suggest an incubation ratio of ca. 8 mmol ligand per gram of nanoparticles provides optimal degrees of ligand surface addition. A gradual decay in nanocrystal luminescence can be observed upon increasing incubating concentrations of 3,4,3-LI(1,2-HOPO), despite a steady increase in the amount of surface-bound ligand, as evidenced by nanoparticle absorption spectra (Figure 2, inset). Concentration

quenching mechanisms between surface-bound ligands may therefore become operative at higher ligand:nanoparticle ratios. Comparisons of the integrated luminescence spectra at this optimal incubation and at the previously used value of 75 mM indicate a luminescence enhancement of roughly 140%. Plots of luminescence intensity as a function of the relative amount of surface-bound ligand (determined using the 320 nm absorption signal of ligand-modified nanoparticle suspensions) reveal a moderate, linear correlation ($R^2 = 0.77$) between the two quantities in the concentration regimes explored (Figure 3).

Internal Quantum Efficiency Calculation

As a complement to our previous report of the external quantum yield in these nanocrystals, we have recently determined the approximate internal quantum yield of europium emission in this system. Measurement of this quantity was achieved using the $^5D_0 \rightarrow {}^7F_1$ transition as basis for calculating total luminescence output. This transition in europium has been generally accepted as purely magnetic-dipole in nature, making it insensitive to the ligand field effects that would otherwise modulate intraband f electronic transitions as a function of chemical environment[73]. In general, the internal quantum yield, Φ_{Int}, is defined as

$$\Phi_{\mathrm{Int}} = \frac{\tau_{obs}}{\tau_{rad}} = \frac{k_{rad}}{k_{obs}} \qquad \text{(equation 3),}$$

where τ_{obs} is the observed luminescence lifetime of some transition and τ_{rad} is the luminescence lifetime in the absence of non-radiative quenching processes.

A value for τ_{rad}, is found through the relation

$$\frac{1}{\tau_{rad}} = An^3\left(\frac{I_{total}}{I_{MD}}\right) \qquad \text{(equation 4),}$$

where A is the spontaneous emission rate of 49.44 s^{-1} for the $^5D_0 \rightarrow {}^7F_1$ emission line, n is the medium's refractive index, I_{total} is the entire integrated luminescence spectrum for Eu^{3+} emission, and I_{MD} is the integrated intensity of europium's magnetic-dipole transition (580 – 600 nm)[73,74]. Applying the refractive index reported for $NaYF_4/NaGdF_4$ host media (1.5)[75,76] to eq. (4) yields a radiative lifetime of 2.9 ms for this transition. Determination of the observed lifetime, τ_{obs}, is commonly found exclusively through the time-resolved measurement of the intense hyperfine emission ($^5D_0 \rightarrow {}^7F_2$) that often dominates europium spectra. However, such an assumption remains valid only for cases where the vast majority of photon emission occurs through this radiative decay channel. This approximation breaks down in cases such as the system investigated here, where spectral integration of nanoparticle luminescence shows that relaxation to the $^7F_2$ state represents only about 60% of the total emission from these samples. This point is highlighted by the marked differences between the luminescence profiles of the $[Eu^{III}$(3,4,3-LI(1,2-HOPO))$]^-$ molecular complex and the modified nanocrystals, where the intensity ratio of the main hypersensitive transition to the other emission lines is far greater in the spectra of the nanocrystals than those of the solution chelate (Figure 4). As a result, it becomes necessary to report k_{obs}, which actually represents the *total* rate of deactivation of the $^5D_0$ excited state (rather than merely its rate of relaxation to any particular ^7F_J multiplet) as the sum of individual rate constants for $^5D_0$ depopulation to the first, second and fourth stark levels of the ^7F ground state ($k_{J=1,2,4}$). We focus on these particular levels as their summed emissions comprise over 90% of the total observed luminescence in these nanoparticles, and their appreciable signal intensities make acquisition of time-resolved luminescence data comparatively easy relative to the low-intensity $^5D_0 \rightarrow {}^7F_{0,3,5,6}$ transitions.

Observed lifetimes for the $^5D_0 \rightarrow {}^7F_{1,2,4}$ transitions were determined from time-resolved luminescence data acquired under ligand excitation at 317 nm. Emission wavelengths of 590 nm, 612 nm and 695 nm were employed for monitoring decay to the $^7F_1$, $^7F_2$ and $^7F_4$ states, respectively. These data reveal all three transitions display bi-exponential decay character. Determination of the physical basis for the presence of multiphase decays in the observed europium emission remains a work in progress, but is possibly the result of different chemical environments seen by bulk Eu^{3+} emitters versus solvent-exposed surface ions. As a result of the multi-phase nature of these decays, rates of deactivation to each ^7F sub-level are expressed as weighted averages of the two distinct rates, k_1 and k_2:

$$\langle k_J \rangle = c_1 k_1 + c_2 k_2 \qquad \text{(equation 5)},$$

where $\langle k_J \rangle$ is the averaged rate for decay to the J^{th} level of the ^7D ground-state manifold, and the weighting coefficients, c_n, are derived from the fractional contribution of each decay phase to the total signal intensity, as found through fitting of the time-resolved luminescence data. The expression $\langle k_1 \rangle + \langle k_2 \rangle + \langle k_4 \rangle$ yields a value for k_{obs}, which we report as 3105 s^{-1} (τ_{obs} = 0.32 ms) for this system; applying this observed lifetime and the natural lifetime to eq. (1) yields a subsequent approximation for the internal quantum efficiency of 11%. The ratio Φ_{Ext}/Φ_{Int} yields a value for the sensitization efficiency. Using the previously reported value of Φ_{Ext} = 0.033 for europium-centered luminescence, we report an estimate for the sensitization efficiency of 0.30.

- *Intersystem Crossing (ISC)*

The efficiency of triplet formation represents a component of the sensitization process, which we have estimated through measurements of the steady-state luminescence spectrum of 3,4,3-LI(1,2-HOPO) bound to undoped, $NaGdF_4$ nanoparticles at liquid-nitrogen temperatures (Figure 5).

Absence of Eu^{3+} doping guarantees that dissipation of the ligand triplet state will occur only through radiative triplet decay to the ligand's ground state or through non-radiative channels, rather than through triplet-donor/metal-acceptor energy transfer, as the first excited state in Gd^{3+} (32,100 cm^{-1}) is too high to be accessed via triplet sensitization by this ligand. Comparison with the room temperature spectrum provides a basis for assigning singlet and triplet states. The room temperature data show a broad luminescence peak with skewed Gaussian character. The ligand emission is sharply resolved into two transitions upon cooling to 77 K. The minor, high-energy peak centered around 415 nm, is assigned as the ligand singlet state (Figure 4). A more intense emission occurs around 525 nm and is attributed to ligand phosphorescence, arising from a triplet state serving as a donor of sufficient energy to overlap with the $^5D_{1,0}$ states (~19,000, 17,250 cm^{-1}) localized on the europium ion. Taking the integrated peak ratios of these two ligand states seen in the cryogenic spectrum provides an approximate value for the efficiency of 3,4,3-LI(1,2-HOPO) triplet state production, for which we find a value of ca. 0.87. This value agrees well with the qualitative observation that ISC in paramagnetic systems containing larger atoms, such as Gd^{3+}, are susceptible to the “heavy atom effect,” which is known to greatly enhance the efficiency of singlet/triplet intersystem crossing[73].

Future Directions

While our most extensive characterizations of ligand-sensitized nanoparticles have focused on europium-doped constructs, attention has now been turned towards the ultimate goal of moving away from merely downshifted luminescence to develop a two-photon nanocrystal downconverter using the platform established in our europium studies. Materials capable of such non-linear photon production have applications in a number of fields, and are especially well

suited for impacting the field of photovoltaics. In the case of downconversion, efficient light absorption at wavelengths where traditional silicon photovoltaics show low photocurrent response, followed by re-emission of multiple lower-energy photons in the infrared regime, holds great potential for designing more efficient solar cells. A great deal of work has been devoted to designing two-photon down-conversion materials using the Tb^{3+}/Yb^{3+} couple[4,5,77–79]. The general principle here relies on crystal lattices or glasses doped with both Tb^{3+} and Yb^{3+}. Following the initial excitation to the terbium ion's $^5D_4$ excited state (~ 20,500 cm^{-1}), its depopulation proceeds through cooperative energy transfer to the $^2F_{5/2}$ level (~ 10,200 cm^{-1}) of neighboring ytterbium species. This two-fold energy mismatch between the terbium and ytterbium excited states allows for the possibility of two-photon emission from Yb^{3+} ions, resulting in near-infrared (NIR) luminescence centered around 980 nm. We have been able to demonstrate that extending our study to the corresponding terbium-doped, rare-earth lattices does result in terbium luminescence (Figure 5), suggesting that it may indeed be possible to construct a bis-doped material where ligand-sensitized Tb^{3+} ion emission is quenched by energy transfer to adjacent ytterbium co-dopants, with subsequent two-photon, NIR emission. This would represent a vast improvement over the red Eu^{3+} emission we've investigated thus far, as silicon photovoltaics (1.1 eV band gap) exhibit peak performance under infrared illumination.

Conclusions

We believe the work being conducted in our group represents a good case study of the value in drawing on the lessons of disparate fields and merging them into a coherent research effort. Our confidence in this approach derives largely from the broader trend established in science over the latter half of the last century to the present, with the burgeoning prominence of

interdisciplinary fields yielding scientific insights that may not have been gained otherwise. The relatively young field of bioinorganic chemistry, a modern synthesis of molecular biology and inorganic chemistry, provides strong validation of this truth. Such an outlook informs our current research strategy, which we view as the convergence of approaches from the generally distinct realms of solid-state photophysics and solution chemistry. The product of this approach has been our realization of colloidal lanthanide materials that represent significant improvements in light absorption and luminescence enhancement for constructs of this nature. Our expectation is that continued adherence to this scientific philosophy will position us to make lasting contributions to the field of spectral conversion and, hopefully, pave the way for the development of ligand sensitized, two-photon down-conversion nanocrystals.

Methods

Synthesis

Europium-doped nanoparticle synthesis and ligand functionalization were performed as previously described[54,70]. Terbium-doped nanoparticles (1% doped) were synthesized using similar procedures. In brief, synthesis proceeded through the addition of 1.98 mL $Gd(CH_3CO_2)_3 \bullet xH_2O$ and 20 μL $Tb(CH_3CO_2)_3 \bullet xH_2O$ (Sigma-Aldrich) to stirring 1-oleic acid (4 mL; Alfa Aesar) and 1-octadecene (6 mL; 90% Sigma-Aldrich) at room temperature. From here, synthesis proceeded as usual according to the procedures of Wang et al[54].

Nanoparticle Luminescence Optimization

Following synthesis, 2.0 mL aliquots of the nanoparticles were precipitated through the addition of 2.0 mL ethanol followed by centrifugation was 13,000 rpm for 10 minutes. Afterward, the supernatant was decanted and the particles were washed through resuspension in 2.0 mL fresh

ethanol via sonication and mechanical mixing by micropipette until a homogenous suspension was formed. This mixture was then centrifuged again for 10 minutes at 13000 rpm, the supernatant decanted, and the particles redispersed in 2.0 mL ethanol. The suspension was divided among 10 Eppendorf microcentrifuge tubes as 200 µL aliquots per tube. Ligand modification reactions were set up by addition of 5, 10, 25, 50, 75 or 100 µL of 75 mM 3,4,3-LI(1,2-HOPO) dissolved in pH 6.5 Hepes buffer to each tube. For lower ligand concentrations explored, a 7.5 mM stock solution of 3,4,3-LI(1,2-HOPO) was used for addition to the tubes in volumes of 0.1, 0.5, 1 and 2 µL. Compensating volumes of buffer were applied to each tube to adjust reaction volumes to a total of 300 µL, with final nanoparticle concentrations of approximately 0.9 mg mL^{-1} $reaction^{-1}$. The reactions were then heated and mixed on a shaker overnight (180 rpm, 60 ºC) to promote 3,4,3-LI(1,2-HOPO) binding to the nanoparticle surfaces. Following incubation, nanoparticles were washed three times in 600 µL ethanol using the procedure described above, before a final resuspension in 600 µL ethanol. Luminescence intensity as a function of ligand surface density was determined using procedures described below.

Steady-State Luminescence

Nanoparticle samples were prepped as dilute colloidal mixtures (A_{500} scatter intensity ~ 0.3) in ethanol to ensure stability of the dispersions during luminescence measurements. Steady-state luminescence spectra were acquired on a Jobin Yvon Horiba Fluorolog system. Luminescence spectra of nanoparticles were collected using a 317 nm excitation wavelength sourced from a xenon arc lamp, 1 nm excitation / 3 nm emission slit settings and 1.0 s integration times at 1 nm resolution. Observation windows of 550-750 nm and 450-650 nm were employed

for the monitoring of europium and terbium luminescence, respectively. Interfering second-harmonic generation originating from the excitation source (~634 nm) was filtered from acquired spectra through the placement of a 400 nm long-pass filter between the sample and detector. Determination of the triplet state of 3,4,3-LI(1,2-HOPO) (bound to $NaGdF_4$ control nanoparticles) proceeded as described elsewhere[70].

Time-Resolved Luminescence

Europium luminescence lifetimes were acquired by monitoring the emission of the $^5D_0 \rightarrow {}^7F_{J=1,2,4}$ transitions at their respective wavelengths of 590, 612, and 695 nm using a Jobin Yvon Horiba Fluorolog spectrometer in time-resolved (MCS lifetime) mode. Experiments were conducted with the following instrument parameters: 317 nm excitation, 14 nm excitation bandpass; 4nm emission bandpass; 10 μs $channel^{-1}$ and 3000 channels $sweep^{-1}$ (30.0 ms observation window). Decay times were extracted via multi-exponential fitting in MATLAB (Supporting Information).

References

(1) Lakshminarayana, G.; Yang, H.; Ye, S.; Liu, Y.; Qiu, J. *J. Mater. Res.* **2008**, *23* (11), 3090–3095.
(2) Eilers, J. J.; Biner, D.; Wijngaarden, J. T. van; Krämer, K.; Güdel, H.-U.; Meijerink, A. *Appl. Phys. Lett.* **2010**, *96* (15), 151106.
(3) Sun, J.; Zhou, W.; Sun, Y.; Zeng, J. *Opt. Commun.* **2013**, *296*, 84–86.
(4) Ye, S.; Katayama, Y.; Tanabe, S. *J. Non-Cryst. Solids* **2011**, *357* (11–13), 2268–2271.
(5) Pan, Z.; Akrobetu, R.; Morgan, S. H. 2013; Vol. 8824, p 88240Z–88240Z–7.
(6) Charbonnière, L. J.; Rehspringer, J.-L.; Ziessel, R.; Zimmermann, Y. *New J. Chem.* **2008**, *32* (6), 1055–1059.
(7) Li, S. W.; Ren, H. J.; Ju, S. G. *J. Nanosci. Nanotechnol.* **2014**, *14* (5), 3677–3682.
(8) Bünzli, J.-C. G. *Chem. Rev.* **2010**, *110* (5), 2729–2755.
(9) Bünzli, J.-C. G.; Piguet, C. *Chem. Soc. Rev.* **2005**, *34* (12), 1048.
(10) Ende, B. M. van der; Aarts, L.; Meijerink, A. *Phys. Chem. Chem. Phys.* **2009**, *11* (47), 11081–11095.
(11) Wang, J.; Deng, R.; MacDonald, M. A.; Chen, B.; Yuan, J.; Wang, F.; Chi, D.; Andy Hor, T. S.; Zhang, P.; Liu, G.; Han, Y.; Liu, X. *Nat. Mater.* **2014**, *13* (2), 157–162.
(12) Chan, E. M.; Levy, E. S.; Cohen, B. E. *Adv. Mater.* **2015**, *27* (38), 5753–5761.
(13) Dupuy, C. G.; Allen, T. L.; Williams, G. M.; Schut, D.; Dupuy, C. G.; Allen, T. L.; Williams, G. M.; Schut, D. *J. Nanotechnol. J. Nanotechnol.* **2014**, *2014*, *2014*, e538163.
(14) Kar, A.; Kundu, S.; Patra, A. *ChemPhysChem* **2015**, *16* (3), 505–521.
(15) Wu, X.; Zhang, Y.; Takle, K.; Bilsel, O.; Li, Z.; Lee, H.; Zhang, Z.; Li, D.; Fan, W.; Duan, C.; Chan, E. M.; Lois, C.; Xiang, Y.; Han, G. *ACS Nano* **2016**, *10* (1), 1060–1066.

(16) Zhou, B.; Shi, B.; Jin, D.; Liu, X. *Nat. Nanotechnol.* **2015**, *10* (11), 924–936.
(17) Choppin, G. R. *J. Alloys Compd.* **1997**, *249* (1–2), 1–8.
(18) Deblonde, G. J.-P.; Sturzbecher-Hoehne, M.; Abergel, R. J. *Inorg. Chem.* **2013**, *52* (15), 8805–8811.
(19) Sturzbecher-Hoehne, M.; Ng Pak Leung, C.; D'Aléo, A.; Kullgren, B.; Prigent, A.-L.; Shuh, D. K.; Raymond, K. N.; Abergel, R. J. *Dalton Trans.* **2011**, *40* (33), 8340.
(20) Blackburn, O. A.; Kenwright, A. M.; Beer, P. D.; Faulkner, S. *Dalton Trans.* **2015**, *44* (45), 19509–19517.
(21) Horrocks, W. D.; Sudnick, D. R. *J. Am. Chem. Soc.* **1979**, *101* (2), 334–340.
(22) Zhou, X.; Zhao, X.; Wang, Y.; Wu, B.; Shen, J.; Li, L.; Li, Q. *Inorg. Chem.* **2014**.
(23) Zheng, W.; Huang, P.; Tu, D.; Ma, E.; Zhu, H.; Chen, X. *Chem. Soc. Rev.* **2014**.
(24) Kataoka, T.; Stekelenburg, A.; Nakanishi, T. M.; Delhaize, E.; Ryan, P. R. *Plant Cell Environ.* **2002**, *25* (3), 453–460.
(25) Weiss, G. B.; Goodman, F. R. *J. Pharmacol. Exp. Ther.* **1976**, *198* (2), 366–374.
(26) Deblonde, G. J.-P.; Sturzbecher-Hoehne, M.; Mason, A. B.; Abergel, R. J. *Metallomics* **2013**, *5* (6), 619–626.
(27) McNemar, C. W.; Horrocks Jr., W. D. *Biochim. Biophys. Acta BBA - Protein Struct. Mol. Enzymol.* **1990**, *1040* (2), 229–236.
(28) Sculimbrene, B. R.; Imperiali, B. *J. Am. Chem. Soc.* **2006**, *128* (22), 7346–7352.
(29) Schmidt, T. W.; Castellano, F. N. *J. Phys. Chem. Lett.* **2014**, 4062–4072.
(30) Ahmed, Z.; Iftikhar, K. *Inorg. Chem.* **2015**, *54* (23), 11209–11225.
(31) Chen, J.; Liu, Y.; Fang, M.; Huang, Z. *Inorg. Chem.* **2014**, *53* (21), 11396–11403.
(32) Liu, Y.; Liu, G.; Wang, J.; Dong, X.; Yu, W. *Inorg. Chem.* **2014**, *53* (21), 11457–11466.
(33) Bünzli, J.-C. G.; Piguet, C. *Chem. Soc. Rev.* **2005**, *34* (12), 1048–1077.
(34) van Wijngaarden, J. T.; Scheidelaar, S.; Vlugt, T. J. H.; Reid, M. F.; Meijerink, A. *Phys. Rev. B* **2010**, *81* (15), 155112.
(35) Martín-Rodríguez, R.; Geitenbeek, R.; Meijerink, A. *J. Am. Chem. Soc.* **2013**, *135* (37), 13668–13671.
(36) Xian-Tao, W.; Jiang-Bo, Z.; Yong-Hu, C.; Min, Y.; Yong, L. *Chin. Phys. B* **2010**, *19* (7), 77804.
(37) Verma, R. K.; Kaur, G.; Rai, A.; Rai, S. B. *Mater. Res. Bull.* **2012**, *47* (11), 3726–3731.
(38) Liang, X. F.; Zhang, Q. Y.; Chen, D. D.; Ji, X. H.; Zhai, J. W. In *Nanoelectronics Conference, 2008. INEC 2008. 2nd IEEE International*; 2008; pp 105–108.
(39) Alombert-Goget, G.; Armellini, C.; Berneschi, S.; Chiappini, A.; Chiasera, A.; Ferrari, M.; Guddala, S.; Moser, E.; Pelli, S.; Rao, D. N.; Righini, G. C. *Opt. Mater.* **2010**, *33* (2), 227–230.
(40) Bünzli, J.-C. G.; Eliseeva, S. V. In *Lanthanide Luminescence*; Hänninen, P., Härmä, H., Eds.; Springer Series on Fluorescence; Springer Berlin Heidelberg, 2010; pp 1–45.
(41) Shavaleev, N. M.; Accorsi, G.; Virgili, D.; Bell, Z. R.; Lazarides, T.; Calogero, G.; Armaroli, N.; Ward, M. D. *Inorg. Chem.* **2005**, *44* (1), 61–72.
(42) Pope, S. J. A.; Coe, B. J.; Faulkner, S.; Bichenkova, E. V.; Yu, X.; Douglas, K. T. *J. Am. Chem. Soc.* **2004**, *126* (31), 9490–9491.
(43) Parker, D.; Dickins, R. S.; Puschmann, H.; Crossland, C.; Howard, J. A. K. *Chem. Rev.* **2002**, *102* (6), 1977–2010.
(44) Fisher, C. M.; Fuller, E.; Burke, B. P.; Mogilireddy, V.; Pope, S. J. A.; Sparke, A. E.; Déchamps-Olivier, I.; Cadiou, C.; Chuburu, F.; Faulkner, S.; Archibald, S. J. *Dalton Trans. Camb. Engl. 2003* **2014**, *43* (25), 9567–9578.
(45) Moore, E. G.; Samuel, A. P. S.; Raymond, K. N. *Acc. Chem. Res.* **2009**, *42* (4), 542–552.
(46) Rajapakse, H. E.; Reddy, D. R.; Mohandessi, S.; Butlin, N. G.; Miller, L. W. *Angew. Chem. Int. Ed.* **2009**, *48* (27), 4990–4992.
(47) Mukherjee, P.; Shade, C. M.; Yingling, A. M.; Lamont, D. N.; Waldeck, D. H.; Petoud, S. *J. Phys. Chem. A* **2011**, *115* (16), 4031–4041.
(48) *Principles of Fluorescence Spectroscopy*; Lakowicz, J. R., Ed.; Springer US: Boston, MA, 2006.
(49) Marcus, R. A.; Sutin, N. *Biochim. Biophys. Acta BBA - Rev. Bioenerg.* **1985**, *811* (3), 265–322.
(50) Banski, M.; Podhorodecki, A.; Misiewicz, J.; Afzaal, M.; Abdelhady, A. L.; O'Brien, P. *J. Mater. Chem. C* **2012**, *1* (4), 801–807.
(51) Wawrzynczyk, D.; Bednarkiewicz, A.; Nyk, M.; Strek, W.; Samoc, M. *J. Nanoparticle Res.* **2013**, *15* (6).

(52) Zou, W.; Visser, C.; Maduro, J. A.; Pshenichnikov, M. S.; Hummelen, J. C. *Nat. Photonics* **2012**, *6* (8), 560–564.
(53) Jang, H. S.; Woo, K.; Lim, K. *Opt. Express* **2012**, *20* (15), 17107.
(54) Wang, F.; Deng, R.; Liu, X. *Nat. Protoc.* **2014**, *9* (7), 1634–1644.
(55) Wang, Z.-L.; Hao, J. H.; Chan, H. L. W. *J. Mater. Chem.* **2010**, *20* (16), 3178–3185.
(56) Zhang, X.; Zhao, Z.; Zhang, X.; Cordes, D. B.; Weeks, B.; Qiu, B.; Madanan, K.; Sardar, D.; Chaudhuri, J. *Nano Res.* **2015**, *8* (2), 636–648.
(57) Chen, G.; Ohulchanskyy, T. Y.; Liu, S.; Law, W.-C.; Wu, F.; Swihart, M. T.; Ågren, H.; Prasad, P. N. *ACS Nano* **2012**, *6* (4), 2969–2977.
(58) Charbonnière, L. J.; Rehspringer, J.-L.; Ziessel, R.; Zimmermann, Y. *New J. Chem.* **2008**, *32* (6), 1055–1059.
(59) Chen, J.; Meng, Q.; May, P. S.; Berry, M. T.; Lin, C. *J. Phys. Chem. C* **2013**, *117* (11), 5953–5962.
(60) Cross, A. M.; May, P. S.; Veggel, F. C. J. M. van; Berry, M. T. *J. Phys. Chem. C* **2010**, *114* (35), 14740–14747.
(61) Ghosh, D.; Luwang, M. N. *RSC Adv.* **2015**, *5* (14), 10468–10478.
(62) Goetz, J.; Nonat, A.; Diallo, A.; Sy, M.; Sera, I.; Lecointre, A.; Lefevre, C.; Chan, C. F.; Wong, K.-L.; Charbonnière, L. J. *ChemPlusChem* **2016**, n/a-n/a.
(63) Irfanullah, M.; Sharma, D. K.; Chulliyil, R.; Chowdhury, A. *Dalton Trans. Camb. Engl. 2003* **2015**, *44* (7), 3082–3091.
(64) Li, S.; Li, X.; Jiang, Y.; Hou, Z.; Cheng, Z.; Ma, P.; Li, C.; Lin, J. *RSC Adv.* **2014**, *4* (98), 55100–55107.
(65) Li, S.; Zhang, X.; Hou, Z.; Cheng, Z.; Ma, P.; Lin, J. *Nanoscale* **2012**, *4* (18), 5619–5626.
(66) Irfanullah, M.; Sharma, D. K.; Chulliyil, R.; Chowdhury, A. *Dalton Trans.* **2015**, *44* (7), 3082–3091.
(67) Janssens, S.; Williams, G. V. M.; Clarke, D. *J. Appl. Phys.* **2011**, *109* (2), 23506.
(68) Zhang, J.; Shade, C. M.; Chengelis, D. A.; Petoud, S. *J. Am. Chem. Soc.* **2007**, *129* (48), 14834–14835.
(69) Nazeeruddin, M. K.; Baranoff, E.; Grätzel, M. *Sol. Energy* **2011**, *85* (6), 1172–1178.
(70) Agbo, P.; Xu, T.; Sturzbecher-Hoehne, M.; Abergel, R. J. *ACS Photonics* **2016**.
(71) Abergel, R. J.; D'Aléo, A.; Ng Pak Leung, C.; Shuh, D. K.; Raymond, K. N. *Inorg. Chem.* **2009**, *48* (23), 10868–10870.
(72) Daumann, L. J.; Tatum, D. S.; Snyder, B. E. R.; Ni, C.; Law, G.; Solomon, E. I.; Raymond, K. N. *J. Am. Chem. Soc.* **2015**, *137* (8), 2816–2819.
(73) Binnemans, K. *Coord. Chem. Rev.* **2015**, *295*, 1–45.
(74) Pacold, J. I.; Tatum, D. S.; Seidler, G. T.; Raymond, K. N.; Zhang, X.; Stickrath, A. B.; Mortensen, D. R. *J. Am. Chem. Soc.* **2014**, *136* (11), 4186–4191.
(75) Yu, D. C.; Huang, X. Y.; Ye, S.; Peng, M. Y.; Zhang, Q. Y.; Wondraczek, L. *Appl. Phys. Lett.* **2011**, *99* (16), 161904.
(76) Zhengwen, Y.; Zhu, K.; Song, Z.; Yu, X.; Zhou, D.; Yin, Z.; Yan, L.; Jianbei, Q. *Appl. Phys. A* **2011**, *103* (4), 995–999.
(77) Zhang, J.; Xia, H.; Jiang, Y.; Yang, S.; Jiang, H.; Chen, B. *IEEE J. Quantum Electron.* **2015**, *51* (6), 1–6.
(78) Chen, D.; Yu, Y.; Wang, Y.; Huang, P.; Weng, F. *J. Phys. Chem. C* **2009**, *113* (16), 6406–6410.
(79) LI, L.; WEI, X.; CHEN, Y.; GUO, C.; YIN, M. *J. Rare Earths* **2012**, *30* (3), 197–201.(1) Lakshminarayana, G.; Yang, H.; Ye, S.; Liu, Y.; Qiu, J. *J. Mater. Res.* **2008**, *23* (11), 3090–3095.
(2) Eilers, J. J.; Biner, D.; Wijngaarden, J. T. van; Krämer, K.; Güdel, H.-U.; Meijerink, A. *Appl. Phys. Lett.* **2010**, *96* (15), 151106.
(3) Sun, J.; Zhou, W.; Sun, Y.; Zeng, J. *Opt. Commun.* **2013**, *296*, 84–86.
(4) Ye, S.; Katayama, Y.; Tanabe, S. *J. Non-Cryst. Solids* **2011**, *357* (11–13), 2268–2271.
(5) Pan, Z.; Akrobetu, R.; Morgan, S. H. 2013; Vol. 8824, p 88240Z–88240Z–7.
(6) Charbonnière, L. J.; Rehspringer, J.-L.; Ziessel, R.; Zimmermann, Y. *New J. Chem.* **2008**, *32* (6), 1055–1059.
(7) Li, S. W.; Ren, H. J.; Ju, S. G. *J. Nanosci. Nanotechnol.* **2014**, *14* (5), 3677–3682.
(8) Bünzli, J.-C. G. *Chem. Rev.* **2010**, *110* (5), 2729–2755.
(9) Bünzli, J.-C. G.; Piguet, C. *Chem. Soc. Rev.* **2005**, *34* (12), 1048.
(10) Ende, B. M. van der; Aarts, L.; Meijerink, A. *Phys. Chem. Chem. Phys.* **2009**, *11* (47), 11081–11095.
(11) Wang, J.; Deng, R.; MacDonald, M. A.; Chen, B.; Yuan, J.; Wang, F.; Chi, D.; Andy Hor, T. S.; Zhang, P.; Liu, G.; Han, Y.; Liu, X. *Nat. Mater.* **2014**, *13* (2), 157–162.

(12) Chan, E. M.; Levy, E. S.; Cohen, B. E. *Adv. Mater.* **2015**, *27* (38), 5753–5761.
(13) Dupuy, C. G.; Allen, T. L.; Williams, G. M.; Schut, D.; Dupuy, C. G.; Allen, T. L.; Williams, G. M.; Schut, D. *J. Nanotechnol. J. Nanotechnol.* **2014**, *2014*, *2014*, e538163.
(14) Kar, A.; Kundu, S.; Patra, A. *ChemPhysChem* **2015**, *16* (3), 505–521.
(15) Wu, X.; Zhang, Y.; Takle, K.; Bilsel, O.; Li, Z.; Lee, H.; Zhang, Z.; Li, D.; Fan, W.; Duan, C.; Chan, E. M.; Lois, C.; Xiang, Y.; Han, G. *ACS Nano* **2016**, *10* (1), 1060–1066.
(16) Zhou, B.; Shi, B.; Jin, D.; Liu, X. *Nat. Nanotechnol.* **2015**, *10* (11), 924–936.
(17) Choppin, G. R. *J. Alloys Compd.* **1997**, *249* (1–2), 1–8.
(18) Deblonde, G. J.-P.; Sturzbecher-Hoehne, M.; Abergel, R. J. *Inorg. Chem.* **2013**, *52* (15), 8805–8811.
(19) Sturzbecher-Hoehne, M.; Ng Pak Leung, C.; D'Aléo, A.; Kullgren, B.; Prigent, A.-L.; Shuh, D. K.; Raymond, K. N.; Abergel, R. J. *Dalton Trans.* **2011**, *40* (33), 8340.
(20) Blackburn, O. A.; Kenwright, A. M.; Beer, P. D.; Faulkner, S. *Dalton Trans.* **2015**, *44* (45), 19509–19517.
(21) Horrocks, W. D.; Sudnick, D. R. *J. Am. Chem. Soc.* **1979**, *101* (2), 334–340.
(22) Zhou, X.; Zhao, X.; Wang, Y.; Wu, B.; Shen, J.; Li, L.; Li, Q. *Inorg. Chem.* **2014**.
(23) Zheng, W.; Huang, P.; Tu, D.; Ma, E.; Zhu, H.; Chen, X. *Chem. Soc. Rev.* **2014**.
(24) Kataoka, T.; Stekelenburg, A.; Nakanishi, T. M.; Delhaize, E.; Ryan, P. R. *Plant Cell Environ.* **2002**, *25* (3), 453–460.
(25) Weiss, G. B.; Goodman, F. R. *J. Pharmacol. Exp. Ther.* **1976**, *198* (2), 366–374.
(26) Deblonde, G. J.-P.; Sturzbecher-Hoehne, M.; Mason, A. B.; Abergel, R. J. *Metallomics* **2013**, *5* (6), 619–626.
(27) McNemar, C. W.; Horrocks Jr., W. D. *Biochim. Biophys. Acta BBA - Protein Struct. Mol. Enzymol.* **1990**, *1040* (2), 229–236.
(28) Sculimbrene, B. R.; Imperiali, B. *J. Am. Chem. Soc.* **2006**, *128* (22), 7346–7352.
(29) Schmidt, T. W.; Castellano, F. N. *J. Phys. Chem. Lett.* **2014**, 4062–4072.
(30) Ahmed, Z.; Iftikhar, K. *Inorg. Chem.* **2015**, *54* (23), 11209–11225.
(31) Chen, J.; Liu, Y.; Fang, M.; Huang, Z. *Inorg. Chem.* **2014**, *53* (21), 11396–11403.
(32) Liu, Y.; Liu, G.; Wang, J.; Dong, X.; Yu, W. *Inorg. Chem.* **2014**, *53* (21), 11457–11466.
(33) Bünzli, J.-C. G.; Piguet, C. *Chem. Soc. Rev.* **2005**, *34* (12), 1048–1077.
(34) van Wijngaarden, J. T.; Scheidelaar, S.; Vlugt, T. J. H.; Reid, M. F.; Meijerink, A. *Phys. Rev. B* **2010**, *81* (15), 155112.
(35) Martín-Rodríguez, R.; Geitenbeek, R.; Meijerink, A. *J. Am. Chem. Soc.* **2013**, *135* (37), 13668–13671.
(36) Xian-Tao, W.; Jiang-Bo, Z.; Yong-Hu, C.; Min, Y.; Yong, L. *Chin. Phys. B* **2010**, *19* (7), 77804.
(37) Verma, R. K.; Kaur, G.; Rai, A.; Rai, S. B. *Mater. Res. Bull.* **2012**, *47* (11), 3726–3731.
(38) Liang, X. F.; Zhang, Q. Y.; Chen, D. D.; Ji, X. H.; Zhai, J. W. In *Nanoelectronics Conference, 2008. INEC 2008. 2nd IEEE International*; 2008; pp 105–108.
(39) Alombert-Goget, G.; Armellini, C.; Berneschi, S.; Chiappini, A.; Chiasera, A.; Ferrari, M.; Guddala, S.; Moser, E.; Pelli, S.; Rao, D. N.; Righini, G. C. *Opt. Mater.* **2010**, *33* (2), 227–230.
(40) Bünzli, J.-C. G.; Eliseeva, S. V. In *Lanthanide Luminescence*; Hänninen, P., Härmä, H., Eds.; Springer Series on Fluorescence; Springer Berlin Heidelberg, 2010; pp 1–45.
(41) Shavaleev, N. M.; Accorsi, G.; Virgili, D.; Bell, Z. R.; Lazarides, T.; Calogero, G.; Armaroli, N.; Ward, M. D. *Inorg. Chem.* **2005**, *44* (1), 61–72.
(42) Pope, S. J. A.; Coe, B. J.; Faulkner, S.; Bichenkova, E. V.; Yu, X.; Douglas, K. T. *J. Am. Chem. Soc.* **2004**, *126* (31), 9490–9491.
(43) Parker, D.; Dickins, R. S.; Puschmann, H.; Crossland, C.; Howard, J. A. K. *Chem. Rev.* **2002**, *102* (6), 1977–2010.
(44) Fisher, C. M.; Fuller, E.; Burke, B. P.; Mogilireddy, V.; Pope, S. J. A.; Sparke, A. E.; Déchamps-Olivier, I.; Cadiou, C.; Chuburu, F.; Faulkner, S.; Archibald, S. J. *Dalton Trans. Camb. Engl. 2003* **2014**, *43* (25), 9567–9578.
(45) Moore, E. G.; Samuel, A. P. S.; Raymond, K. N. *Acc. Chem. Res.* **2009**, *42* (4), 542–552.
(46) Rajapakse, H. E.; Reddy, D. R.; Mohandessi, S.; Butlin, N. G.; Miller, L. W. *Angew. Chem. Int. Ed.* **2009**, *48* (27), 4990–4992.

(47) Mukherjee, P.; Shade, C. M.; Yingling, A. M.; Lamont, D. N.; Waldeck, D. H.; Petoud, S. *J. Phys. Chem. A* **2011**, *115* (16), 4031–4041.
(48) *Principles of Fluorescence Spectroscopy*; Lakowicz, J. R., Ed.; Springer US: Boston, MA, 2006.
(49) Marcus, R. A.; Sutin, N. *Biochim. Biophys. Acta BBA - Rev. Bioenerg.* **1985**, *811* (3), 265–322.
(50) Banski, M.; Podhorodecki, A.; Misiewicz, J.; Afzaal, M.; Abdelhady, A. L.; O'Brien, P. *J. Mater. Chem. C* **2012**, *1* (4), 801–807.
(51) Wawrzynczyk, D.; Bednarkiewicz, A.; Nyk, M.; Strek, W.; Samoc, M. *J. Nanoparticle Res.* **2013**, *15* (6).
(52) Zou, W.; Visser, C.; Maduro, J. A.; Pshenichnikov, M. S.; Hummelen, J. C. *Nat. Photonics* **2012**, *6* (8), 560–564.
(53) Jang, H. S.; Woo, K.; Lim, K. *Opt. Express* **2012**, *20* (15), 17107.
(54) Wang, F.; Deng, R.; Liu, X. *Nat. Protoc.* **2014**, *9* (7), 1634–1644.
(55) Wang, Z.-L.; Hao, J. H.; Chan, H. L. W. *J. Mater. Chem.* **2010**, *20* (16), 3178–3185.
(56) Zhang, X.; Zhao, Z.; Zhang, X.; Cordes, D. B.; Weeks, B.; Qiu, B.; Madanan, K.; Sardar, D.; Chaudhuri, J. *Nano Res.* **2015**, *8* (2), 636–648.
(57) Chen, G.; Ohulchanskyy, T. Y.; Liu, S.; Law, W.-C.; Wu, F.; Swihart, M. T.; Ågren, H.; Prasad, P. N. *ACS Nano* **2012**, *6* (4), 2969–2977.
(58) Charbonnière, L. J.; Rehspringer, J.-L.; Ziessel, R.; Zimmermann, Y. *New J. Chem.* **2008**, *32* (6), 1055–1059.
(59) Chen, J.; Meng, Q.; May, P. S.; Berry, M. T.; Lin, C. *J. Phys. Chem. C* **2013**, *117* (11), 5953–5962.
(60) Cross, A. M.; May, P. S.; Veggel, F. C. J. M. van; Berry, M. T. *J. Phys. Chem. C* **2010**, *114* (35), 14740–14747.
(61) Ghosh, D.; Luwang, M. N. *RSC Adv.* **2015**, *5* (14), 10468–10478.
(62) Goetz, J.; Nonat, A.; Diallo, A.; Sy, M.; Sera, I.; Lecointre, A.; Lefevre, C.; Chan, C. F.; Wong, K.-L.; Charbonnière, L. J. *ChemPlusChem* **2016**, n/a-n/a.
(63) Irfanullah, M.; Sharma, D. K.; Chulliyil, R.; Chowdhury, A. *Dalton Trans. Camb. Engl. 2003* **2015**, *44* (7), 3082–3091.
(64) Li, S.; Li, X.; Jiang, Y.; Hou, Z.; Cheng, Z.; Ma, P.; Li, C.; Lin, J. *RSC Adv.* **2014**, *4* (98), 55100–55107.
(65) Li, S.; Zhang, X.; Hou, Z.; Cheng, Z.; Ma, P.; Lin, J. *Nanoscale* **2012**, *4* (18), 5619–5626.
(66) Irfanullah, M.; Sharma, D. K.; Chulliyil, R.; Chowdhury, A. *Dalton Trans.* **2015**, *44* (7), 3082–3091.
(67) Janssens, S.; Williams, G. V. M.; Clarke, D. *J. Appl. Phys.* **2011**, *109* (2), 23506.
(68) Zhang, J.; Shade, C. M.; Chengelis, D. A.; Petoud, S. *J. Am. Chem. Soc.* **2007**, *129* (48), 14834–14835.
(69) Nazeeruddin, M. K.; Baranoff, E.; Grätzel, M. *Sol. Energy* **2011**, *85* (6), 1172–1178.
(70) Agbo, P.; Xu, T.; Sturzbecher-Hoehne, M.; Abergel, R. J. *ACS Photonics* **2016,** 3(4), 547–552
(71) Abergel, R. J.; D'Aléo, A.; Ng Pak Leung, C.; Shuh, D. K.; Raymond, K. N. *Inorg. Chem.* **2009**, *48* (23), 10868–10870.
(72) Daumann, L. J.; Tatum, D. S.; Snyder, B. E. R.; Ni, C.; Law, G.; Solomon, E. I.; Raymond, K. N. *J. Am. Chem. Soc.* **2015**, *137* (8), 2816–2819.
(73) Binnemans, K. *Coord. Chem. Rev.* **2015**, *295*, 1–45.
(74) Pacold, J. I.; Tatum, D. S.; Seidler, G. T.; Raymond, K. N.; Zhang, X.; Stickrath, A. B.; Mortensen, D. R. *J. Am. Chem. Soc.* **2014**, *136* (11), 4186–4191.
(75) Yu, D. C.; Huang, X. Y.; Ye, S.; Peng, M. Y.; Zhang, Q. Y.; Wondraczek, L. *Appl. Phys. Lett.* **2011**, *99* (16), 161904.
(76) Zhengwen, Y.; Zhu, K.; Song, Z.; Yu, X.; Zhou, D.; Yin, Z.; Yan, L.; Jianbei, Q. *Appl. Phys. A* **2011**, *103* (4), 995–999.
(77) Zhang, J.; Xia, H.; Jiang, Y.; Yang, S.; Jiang, H.; Chen, B. *IEEE J. Quantum Electron.* **2015**, *51* (6), 1–6.
(78) Chen, D.; Yu, Y.; Wang, Y.; Huang, P.; Weng, F. *J. Phys. Chem. C* **2009**, *113* (16), 6406–6410.
(79) LI, L.; WEI, X.; CHEN, Y.; GUO, C.; YIN, M. *J. Rare Earths* **2012**, *30* (3), 197–201.

Acknowledgements

The authors would like to thank Dr. Joseph Pacold for his helpful insights regarding internal quantum yield determination, and Tao Xu for his help with TEM imaging.

This work was supported by the U.S. Department of Energy, Office of Science, Office of Basic Energy Sciences, Chemical Sciences, Geosciences, and Biosciences Division at the Lawrence Berkeley National Laboratory under Contract DE-AC02-05CH11231. RJA is the recipient of a U.S. Department of Energy, Office of Science Early Career Award.
U.S. Department of Energy, Office of Science Early Career Award.

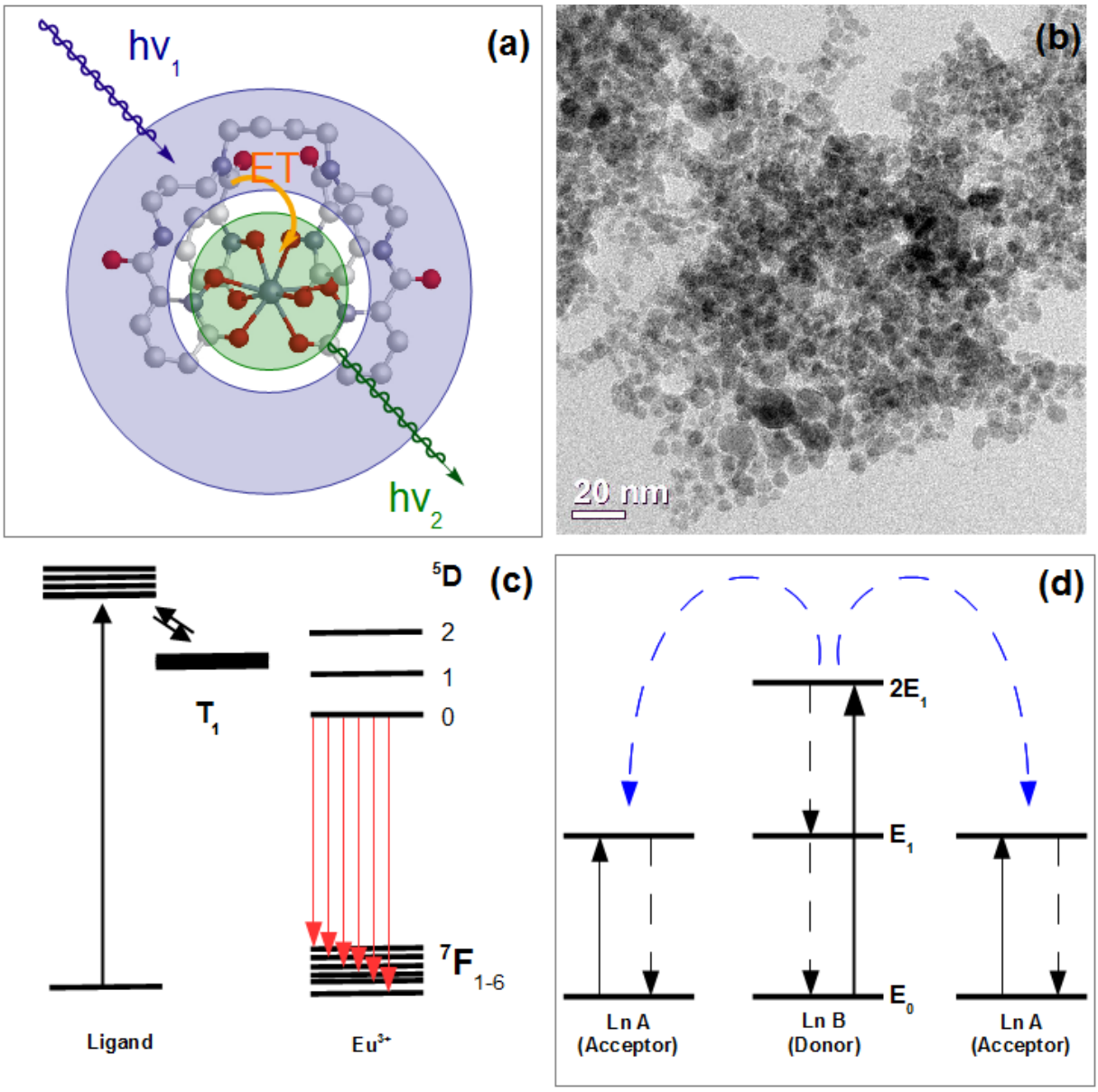

Figure 1

A) A general depiction of ligand-sensitized lanthanide emission. B) From ref. (70): Transmission electron micrograph of hexagonal $NaGd_{1-x}Eu_xF_4$ nanoparticles capped with the ligand 3,4,3-LI(1,2-HOPO). C) A simplified Jablonski diagram of europium sensitization by 3,4,3-LI(1,2-HOPO). D) A generic cooperative energy transfer downconversion scheme. E) The molecular structure of the photosensitizer 3,4,3-LI(1,2-HOPO).

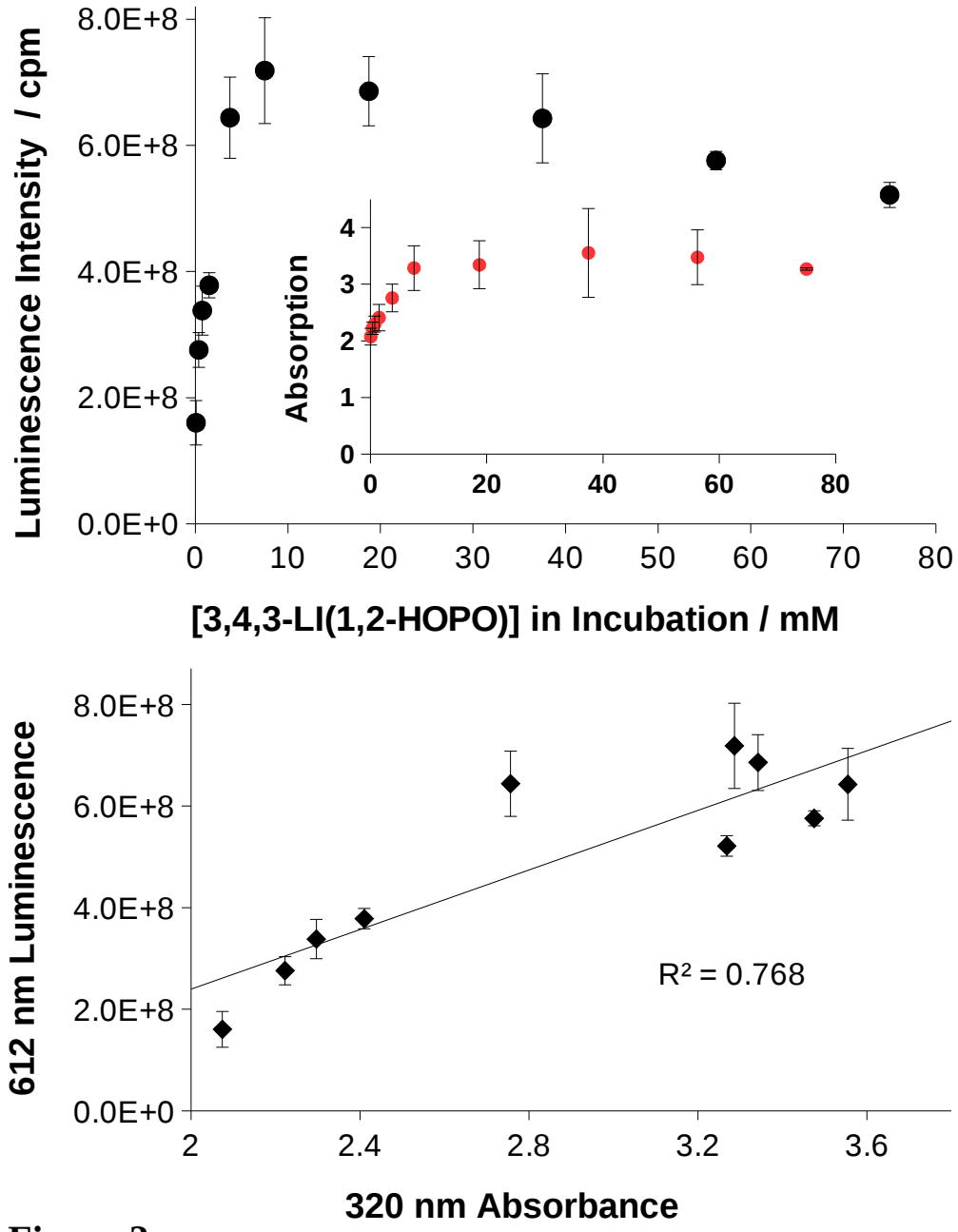

Figure 2

(a) Dependence of nanoparticle luminescence intensity (317 nm excitation wavelength) as a function of the concentration of 3,4,3-LI(1,2-HOPO) used in incubations. The slow drop in intensity at much higher ligand concentrations is attributed to concentration quenching between bound 343 moieties at nanocrystalline surfaces. (Inset) Increasing the ligand solution concentration results in an increase in its localization at the nanoparticle surface before plateauing around 10 mM, as shown through monitoring the ligand 320 nm absorption signal (normalized relative to scatter at 500 nm).

(b) Correlation between relative measures of bound ligand, found through 320 nm absorbance of 3,4,3-LI(1,2-HOPO), and peak nanoparticle luminescence at 612 nm, is approximately linear.

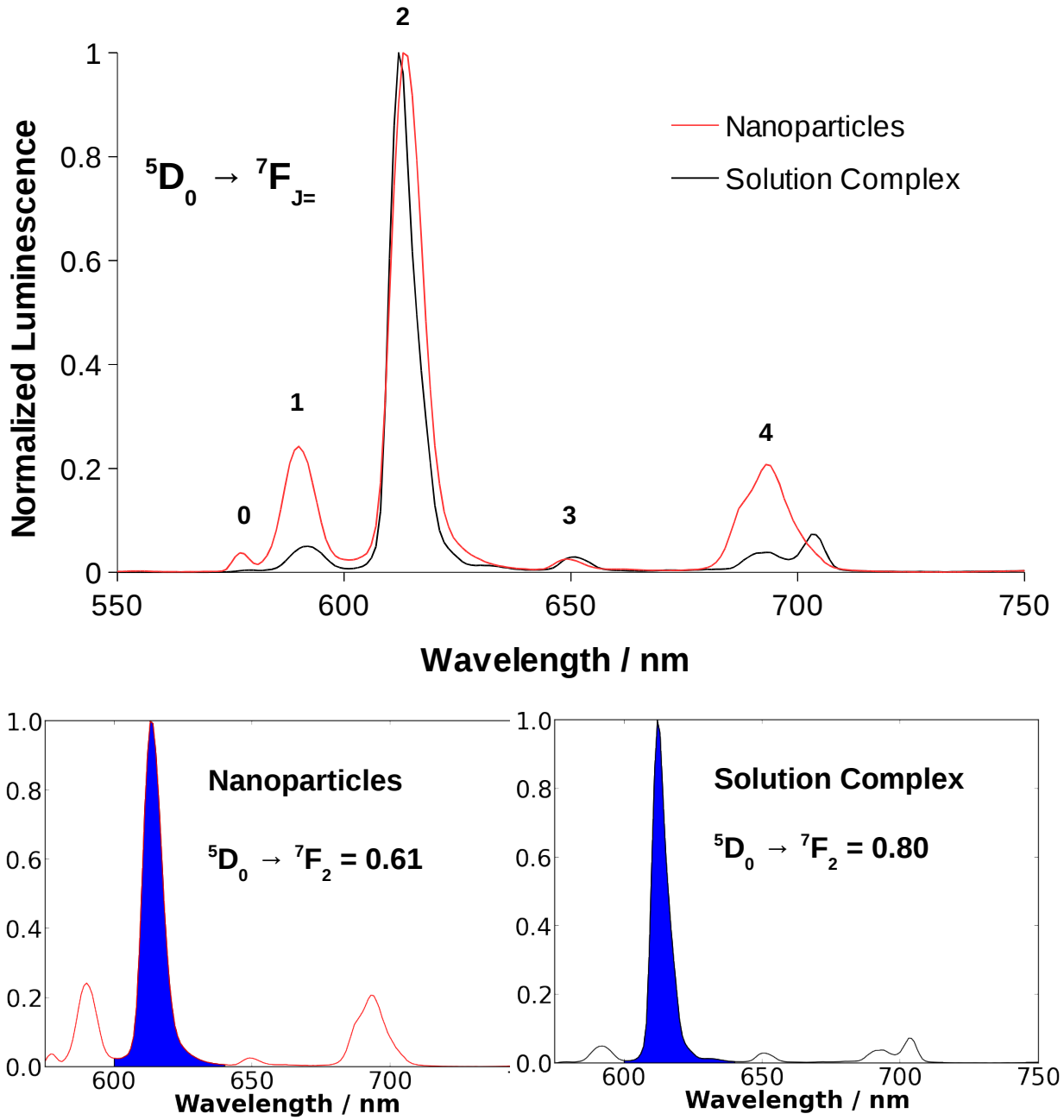

Figure 3

Top panel: Normalized luminescence of ligand-modified, Eu-doped nanoparticles and the Eu(III)-3,4,3-LI(1,2-HOPO) solution complex in ethanol.

Bottom Panel: Integrated spectra indicate that the main transition at 612 nm (integration bounds 600-640 nm) constitutes a much smaller portion of total photon emission in the nanoparticles (ca. 61%) compared to the metal-ligand complex (ca. 80%).

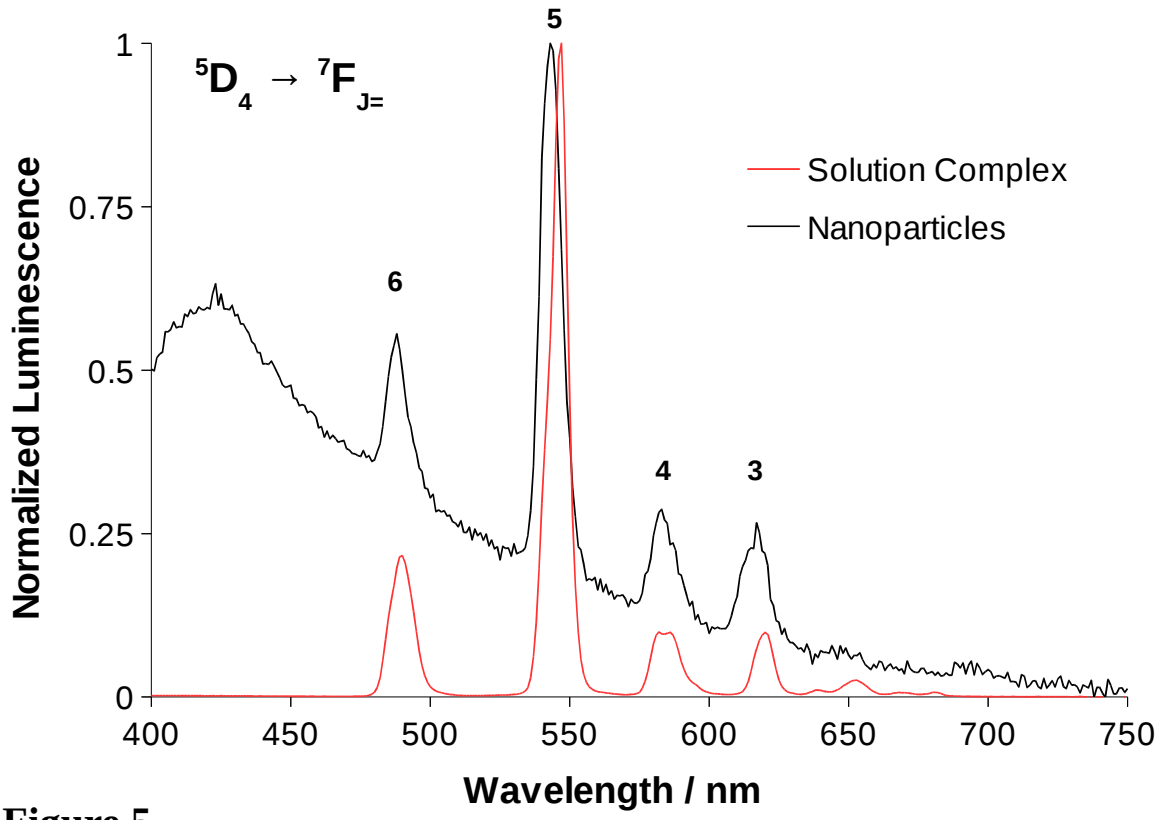

Figure 5

Luminescence spectra of terbium-doped $NaGdF_4$ nanoparticles sensitized by 3,4,3-LI(1,2-HOPO) (black) and the terbium solution complex normalized to the peak ($^5D_4 \rightarrow {}^7F_5$) transition. Nanoparticle emission marks the superposition of terbium luminescence and a broad Raman signature previously ascribed to residual oleate ligands on the nanoparticle surface.

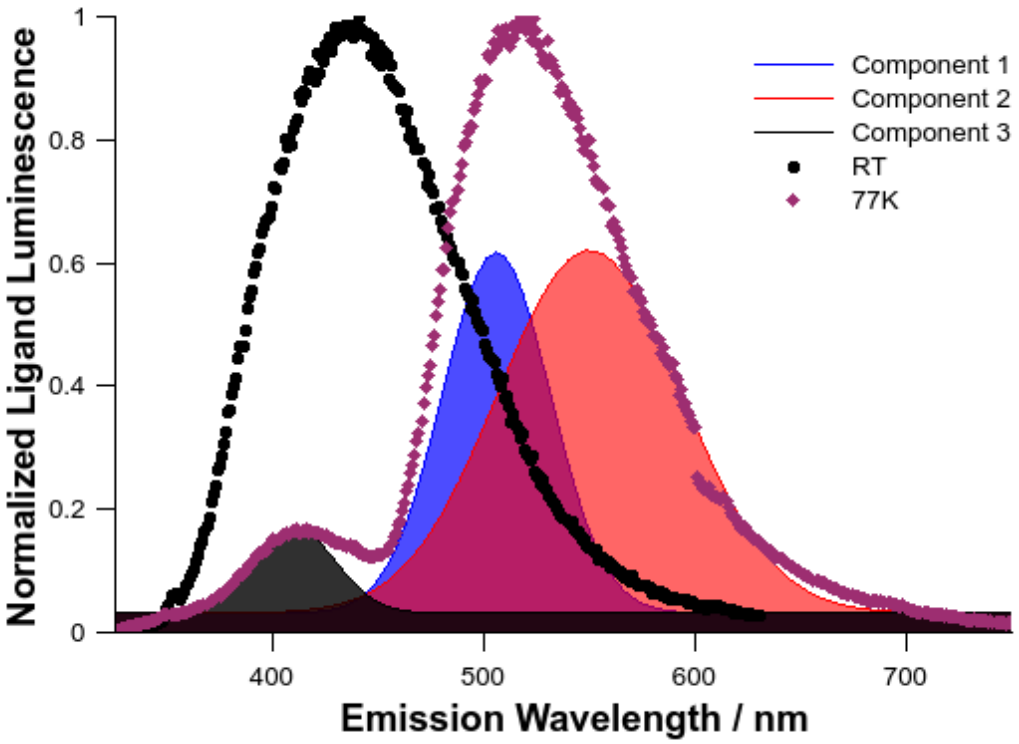

Figure 4

Adapted from (70). Luminescence spectra of Gd(III)-3,4,3-LI(1,2-HOPO) in ethanol at room temperature (black dots) and in a 77 K glass (violet diamonds). The room temperature spectrum represents the coalescence of singlet and triplet states into a skewed Gaussian dominated by singlet character. The 77 K spectrum allows for assignment of the peak at 525 nm to the ligand triplet excited state, with a minor contribution from the ligand singlet visible at 415 nm. Integration of these peaks in the cooled spectrum allows for estimation of the efficiency for triplet production via intersystem crossing.

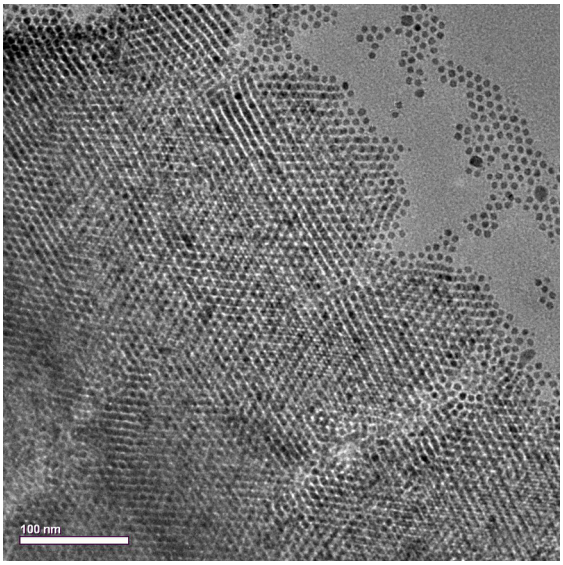

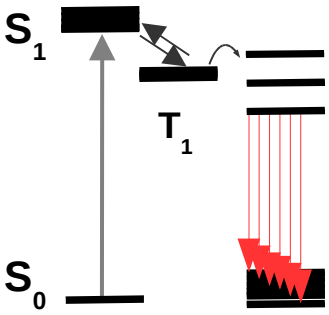

Ligand Nanocrystal